Technology

Molecular Cell

Monitoring Mitochondrial Pyruvate Carrier Activity in Real Time Using a BRET-Based Biosensor: Investigation of the Warburg Effect

Graphical Abstract

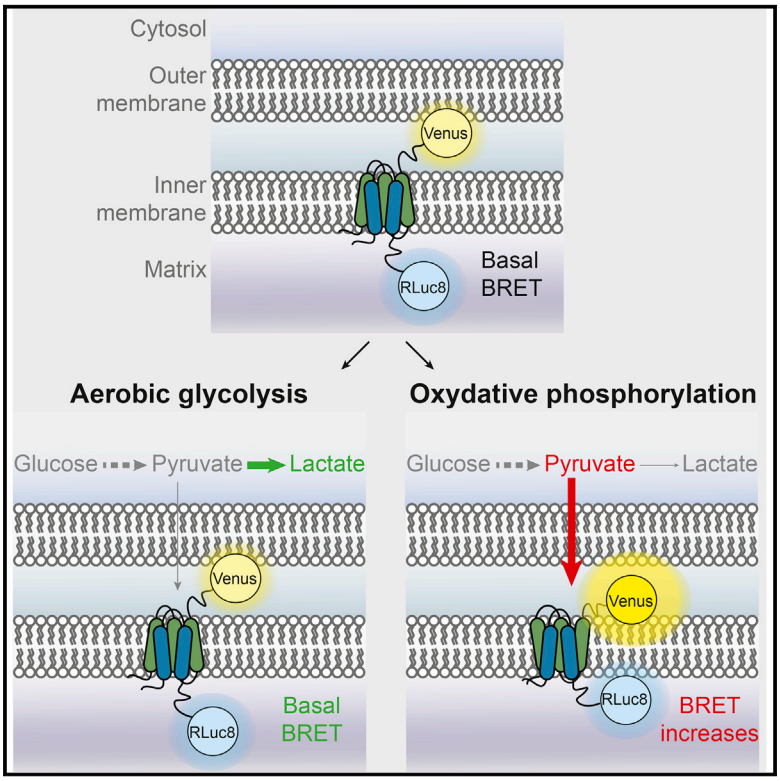

Authors

Vincent Compan, Sandra Pierredon, Benoît Vanderperre, ..., Nicola Zamboni, Jacques Pouyssegur, Jean-Claude Martinou

Correspondence

jean-claude.martinou@unige.ch

In Brief

Current techniques for monitoring influx of pyruvate into mitochondria provide only an indirect measure of mitochondrial pryuvate carrier (MPC) activity. Compan et al. have engineered a biosensor that enables monitoring MPC activity in real time to investigate metabolism in living cells.

Highlights

- RESPYR is a genetically encoded biosensor based on bioluminescence energy transfer
- RESPYR enables monitoring mitochondrial pyruvate carrier activity in real time
- RESPYR enables analysis of the mitochondrial pyruvate carrier in single cells
- RESPYR provides a non-invasive technology to monitor cellular energy metabolism

Compan et al., 2015, Molecular Cell *59*, 491–501
August 6, 2015
http://dx.doi.org/10.1016/j.molcel.2015.06.035

CellPress

Molecular Cell
Technology

Monitoring Mitochondrial Pyruvate Carrier Activity in Real Time Using a BRET-Based Biosensor: Investigation of the Warburg Effect

Vincent Compan,[1,2] Sandra Pierredon,[1] Benoît Vanderperre,[1] Petra Krznar,[3] Ibtissam Marchiq,[4] Nicola Zamboni,[3] Jacques Pouyssegur,[4,5] and Jean-Claude Martinou[1,*]
[1]Department of Cell Biology, University of Geneva, 30 quai Ernest-Ansermet, 1211 Genève 4, Switzerland
[2]Institut de Génomique Fonctionnelle Labex ICST; INSERM U661, CNRS UMR5203; Université Montpellier, 141, rue de la Cardonille, 34094 Montpellier cedex 5, France
[3]ETH Zurich, Institute of Molecular Systems Biology Auguste-Piccard-Hof 1, 8093 Zurich, Switzerland
[4]Institute for Research on Cancer and Aging of Nice (IRCAN), University of Nice Sophia Antipolis, Centre A. Lacassagne, 06189 Nice, France
[5]Centre Scientifique de Monaco, 8, Quai Antoine 1er MC, 98000, Monaco
*Correspondence: jean-claude.martinou@unige.ch
http://dx.doi.org/10.1016/j.molcel.2015.06.035

SUMMARY

The transport of pyruvate into mitochondria requires a specific carrier, the mitochondrial pyruvate carrier (MPC). The MPC represents a central node of carbon metabolism, and its activity is likely to play a key role in bioenergetics. Until now, investigation of the MPC activity has been limited. However, the recent molecular identification of the components of the carrier has allowed us to engineer a genetically encoded biosensor and to monitor the activity of the MPC in real time in a cell population or in a single cell. We report that the MPC activity is low in cancer cells, which mainly rely on glycolysis to generate ATP, a characteristic known as the Warburg effect. We show that this low activity can be reversed by increasing the concentration of cytosolic pyruvate, thus increasing oxidative phosphorylation. This biosensor represents a unique tool to investigate carbon metabolism and bioenergetics in various cell types.

INTRODUCTION

Cells can undergo dramatic variations in energetic metabolism depending on their nature, activity, and microenvironment. In this respect, cancer cells represent a good example of metabolic adaptation. Many cancer cells dispense completely with ATP generation through the highly efficient mitochondrial respiratory pathway and rely on glycolysis for ATP generation even when growing in the presence of oxygen. This process was originally described in the early part of the last century by Otto Warburg and has since become known as the Warburg effect (Bayley and Devilee, 2012; Hsu and Sabatini, 2008). Though less efficient for energy production, this type of metabolism provides an abundant supply of carbon building blocks necessary for the increased demands of rapidly expanding tissues and tumors (DeBerardinis et al., 2008; Vander Heiden et al., 2009). As a potential strategy for cancer therapy, drugs that enhance mitochondrial ATP production through respiration have been proposed and have shown promising results (Jang et al., 2013; Michelakis et al., 2010). However, the mechanisms that underlie metabolic reprogramming between oxidative phosphorylation (OXPHOS) and aerobic glycolysis are diverse and remain incompletely elucidated (Cairns et al., 2011; Locasale and Cantley, 2011).

A key intermediate in regulating cellular energy metabolism is pyruvate, the end product of glycolysis. Pyruvate can either be reduced in the cytoplasm by lactate dehydrogenase (LDH), leading to production of lactate, a key step that refuels glycolysis, or it can be transported into mitochondria as the primary substrate for the citric acid cycle, leading to complete oxidation and highly efficient ATP generation. Thus, control over the intracellular fate of pyruvate emerges as a critical decision point in regulating energy metabolism,

40 years ago, Papa et al. (1971), based on a series of biochemical experiments, postulated the existence of a mitochondrial pyruvate carrier (MPC) that allows pyruvate entry into the mitochondrial matrix. However, the molecular identity of the MPC remained elusive. It was finally revealed by two groups in 2012 (Bricker et al., 2012; Herzig et al., 2012) and shown to be highly conserved throughout evolution. In mammals, the MPC appears to be composed of two paralogous subunits, MPC1 and MPC2, that interact to form a heteromeric complex. Located in the inner mitochondrial membrane, the MPC is strategically positioned at the intersection between glycolysis in the cytosol and OXPHOS in the mitochondria. We anticipate that its function must be tightly and specifically regulated in the control of cell homeostasis and cell fate (Vanderperre et al., 2015). Assessment of the activity of the MPC is therefore of key importance for our understanding of the regulation of cell metabolism.

DESIGN

Current techniques for monitoring influx of pyruvate into mitochondria are limited in their spatio-temporal resolution and

provide only an indirect measure of the MPC activity. For example, import of radiolabelled pyruvate does not allow monitoring of the MPC activity in real time and in situ. Alternatively, procedures that measure pyruvate-driven oxygen consumption in real time do not represent a direct quantification of the activity of MPC since many steps are required for pyruvate oxidation following its import into the mitochondria. Furthermore, flux metabolomics (Hiller and Metallo, 2013), including the use of hyperpolarized ^{13}C-enriched substrates (Yang et al., 2014a) that define a precise metabolic phenotype of cells, do not allow direct assessment of the MPC activity. In addition, all of these different approaches are time and cell consuming.

The recent molecular characterization of the MPC provided new possibilities to investigate its activity, and with this aim in mind we have engineered a genetically encoded biosensor based on bioluminescence resonance energy transfer (BRET), which we called RESPYR (for REporter Sensitive to PYRuvate). By monitoring the changes in BRET in different cell types and under different conditions, we have been able to monitor the activity of the MPC in real time with a high temporal resolution. Using RESPYR, we have compared beta pancreatic cells in which mitochondrial OXPHOS is highly active, with a variety of cancer cells in which ATP is produced mainly through aerobic glycolysis. Similar BRET changes were recorded in all cell types exposed to pyruvate, whereas in the presence of glucose, only the beta pancreatic cells showed MPC activity. However, we found that indirectly increasing the intracellular pyruvate concentration in cancer cells by inhibition of lactate export via the monocarboxylate transporter (MCT) significantly increased MPC activity and cell respiration when cells were exposed to glucose. These results therefore suggest the possibility of using RESPYR in high-throughput screening mode to identify molecules capable of modulating MPC activity. Such molecules could provide a promising approach to cancer therapy.

RESULTS

A BRET Sensor to Detect MPC Activity

To monitor the activity of the MPC in real time, we assumed that transport of pyruvate would induce reversible changes in its conformation. To test this, we constructed a genetically encoded biosensor based on BRET in which MPC1 and MPC2 were modified by C-terminal fusion to either the donor group RLuc8 (a variant of *Renilla* luciferase) or the acceptor group Venus (a variant of yellow fluorescent protein) (Figure 1A). We hypothesized that conformational changes during pyruvate binding and/or transport would cause a change in the energy transfer between MPC1 and MPC2, which may allow us to monitor MPC activity in real time by measuring the variation in BRET.

We first confirmed that the properties of the tagged proteins were similar to those of endogenous MPC regarding subcellular localization (Figure 1B), expression levels (Figure S1A), molecular assembly (Figure S1B), and function (Figure 1C and Figure S1C); furthermore, we showed that stable expression of MPC1-Venus and MPC2-Rluc8 in HEK293 cells did not alter either proliferation or oxygen consumption (Figures S1D and S1E). We next checked the interaction between MPC proteins in HEK293 cells by recording the BRET signals in the presence of the luciferase substrate coelenterazine h (Figure 1D). When cells were co-transfected with a fixed amount of MPC1-RLuc8 together with increasing amounts of the MPC2-Venus (Figure 1D, left panel), a high and specific BRET signal could be measured as shown by saturation of the signal when high amounts of MPC2-Venus proteins were present. No evidence for MPC1 homomerization or for interaction with the negative control (the unfused Venus construct) could be detected, as shown by the linear and low increase in the BRET signal with increasing amounts of the acceptors. In the converse experiment in which cells were transfected with a constant amount of MPC2-RLuc8 (Figure 1D, right panel), a specific and saturable BRET signal with MPC1-Venus was again detected. Interestingly, in this case a similar signal was also measured in the presence of MPC2-Venus, indicating that MPC2 was capable of homomerization. Altogether, these results show that MPC1 and MPC2 were able to heteromerize in HEK293 cells and that homomers of MPC2 were also able to form. We then assessed the conformational changes of the MPC when cells were exposed to various stimuli (Figure 1E). In the presence of PBS alone, the basal BRET signal remained stable for at least the 20 min duration of the experiment. Incubation of the cells in 5 mM pyruvate led to a rapid increase in BRET (Figure 1E and Figure S1F), indicating that the binding and/or transport of pyruvate caused a conformational shift in the carrier complex, bringing the BRET acceptor and donor groups into a closer proximity. The BRET changes remained stable while pyruvate was present. Similar results were found for both configurations of the heteromeric MPC1/MPC2 complexes. In contrast, no pyruvate-induced conformational shift was observed for MPC2 homomers (Figure 1E), in agreement with our previous results showing that only MPC1/MPC2 heteromeric complexes are functional (Herzig et al., 2012). In the work reported here, all subsequent BRET experiments have been performed using the combination of MPC2-RLuc8 and MPC1-Venus. This biosensor was named RESPYR (for REporter Sensitive to PYRuvate).

Functional Properties of RESPYR

To investigate the selectivity of RESPYR, various metabolites including pyruvate lactate, malate, and citrate were added to RESPYR-expressing cells after permeabilization to ensure access to the biosensor. Only pyruvate was able to activate RESPYR in HEK293 cells (Figure 2A) and other cell lines (Figure S2), with EC_{50}s ranging between 225 μM and 452 μM (Figure 2B). For further validation of RESPYR, we used the monocarboxylate transporter 1 and 2 (MCT) inhibitor AR-C155858 to block pyruvate import at the plasma membrane into HEK293 cells. Pre-incubation of cells with AR-C155858 prevented the BRET increase induced by pyruvate (Figure 2C, left panel), while addition of the compound 10 min after pyruvate stimulation (Figure 2C, right panel) led to a progressive decrease in the BRET signal back to the basal level. Thus, changes in MPC activity as measured by the BRET response are fully reversible.

Glucose Consumption Induces MPC Activity in a Beta Pancreatic Cell Line, but Not in Cancer Cells

Because of the key location of MPC at the interface between glycolysis and OXPHOS (Figure 3A), RESPYR provides a novel

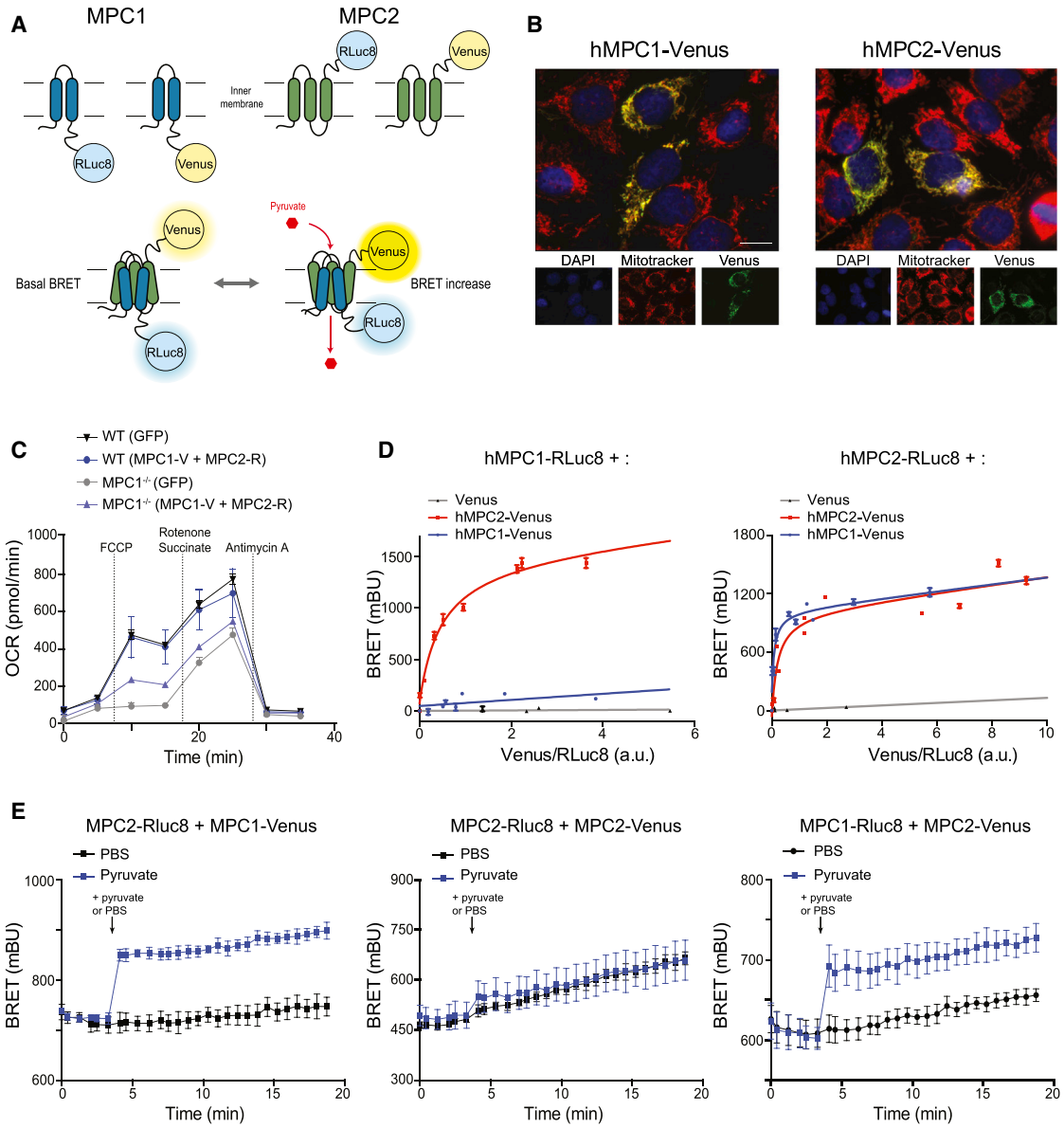

Figure 1. RESPYR, a BRET-Based Sensor to Monitor MPC Activity

(A) Schematic representations showing MPC subunits tagged with either RLuc8 or Venus (top panel) according to the recently described membrane topology of MPC1 and MPC2 (Bender et al., 2015), and pyruvate-induced changes in MPC conformation leading to increase in BRET signal (bottom panel).

(B) Representative images showing the subcellular localization of hMPC1 and hMPC2 tagged with Venus. 2 days after transfection with either MPC1-Venus or MPC2-Venus (green), HeLa cells were stained for mitochondria using Mitotracker (red) and for nuclei with Dapi (blue). Scale bar, 10 μm.

(C) MPC1-Venus and MPC2-RLuc8 are functional and able to transport pyruvate into the mitochondrial matrix. Representative experiment showing the oxygen consumption rate (OCR) of MEFs from either wild-type (WT) or MPC1$^{-/-}$ mice transfected with either GFP or MPC1-Venus and MPC2-RLuc8 (MPC1-V + MPC2-R). Oxygen consumption profiles were determined on XF PMP permeabilized cells in the presence of pyruvate as the only carbon source.

(D) BRET saturation curves for HEK293 cells transfected with a constant amount of either hMPC1-RLuc8 (left panel) or hMPC2-RLuc8 (right panel) and increasing amounts of hMPC1-Venus (blue), hMPC2-Venus (red), or the BRET acceptor Venus alone (black). a.u. = arbitrary unit calculated as described in Experimental Procedures. Data are mean ± SEM of three independent experiments.

(E) BRET kinetics obtained in HEK293 cells transfected with different combinations of hMPC1- and hMPC2-tagged BRET donors and acceptors as indicated. Cells were stimulated with either PBS (black) or 5 mM pyruvate (blue) at the times indicated by the arrows. Data shown are mean ± SEM from one experiment with 4 wells for each data point and are representative of three independent experiments.

See also Figure S1.

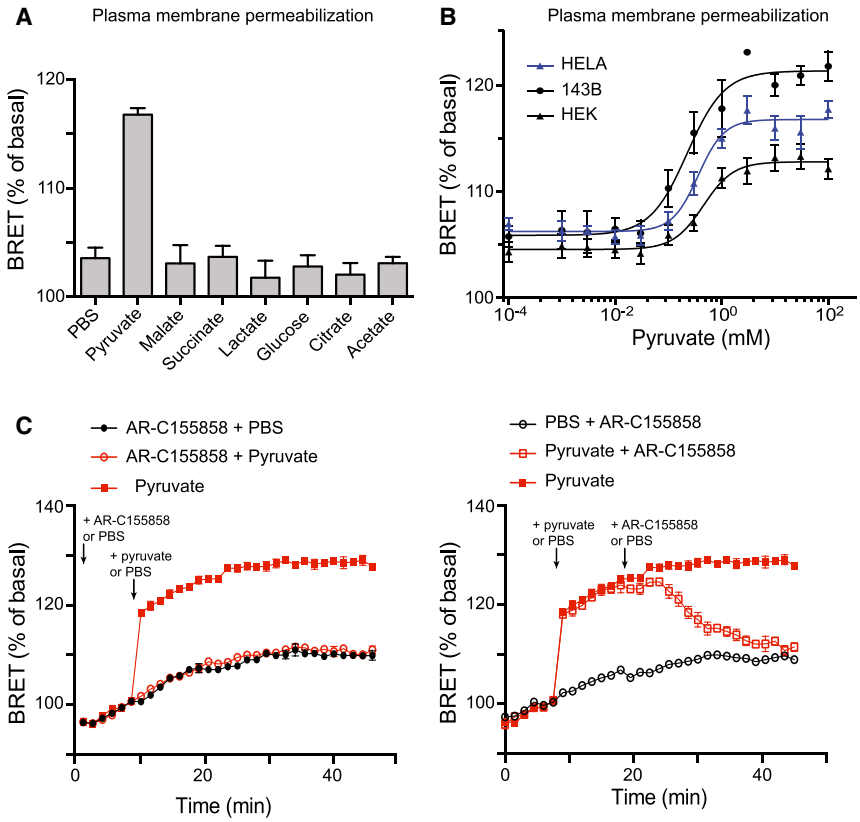

Figure 2. Functional Properties of RESPYR

(A) BRET variation in HEK293 cells transfected with the RESPYR components, permeabilized with 1 nM XPMP, and exposed to different substrates (all present at 20 mM, with the exception of pyruvate present at 5 mM). BRET signals were measured 10 min after stimulation and represented as the percentage of the basal BRET signal.

(B) Dose response of BRET to increasing amounts of pyruvate. Cells were permeabilized as described in (A). The EC_{50} values for HeLa, 143B, and HEK293 were 0.362 mM, 0.225 mM, and 0.452 mM, respectively, with 95% confidence limits ranging from 0.248 to 0.528 mM, 0.12 to 0.398 mM, and 0.249 to 0.822 mM, respectively. Data shown in (A) and (B) are mean ± SEM of three independent experiments.

(C) BRET kinetics in HEK293 cells expressing the RESPYR components and stimulated with either PBS (black) or 5 mM pyruvate (red). At the times indicated by arrows, cells were exposed to AR-C155858 (empty symbols). AR-C155858 was added before (left panel) or after (right panel) stimulation with PBS or pyruvate. Data are mean ± SEM from one experiment with 4 wells for each data point and are representative of three independent experiments.

See also Figure S2.

means to monitor changes in cellular metabolism under various growth conditions and in diverse cell types. As a proof of concept, RESPYR was expressed in either rat pancreatic β cells (INS-1E) in which ATP is predominantly produced through OXPHOS (Spacek et al., 2008) or HEK293 cells in which glycolysis provides the main source of energy (Dietmair et al., 2012; Henry et al., 2011). In both cell types, addition of pyruvate induced a similar rapid increase in BRET signal (Figure 3B), showing that RESPYR was expressed and functional. In contrast, when glucose was added as the sole energy source, the cells responded quite differently. In INS-1E cells, the BRET signal increased progressively over several minutes, presumably the time required to produce pyruvate by glycolysis, and reached a plateau when the BRET signal approached 50% of BRET signal recorded in the presence of pyruvate (Figure 3B, left panel). This increase was completely reversed by addition of 2-deoxyglucose (Figure S3A), a glucose analog that inhibits glycolysis (Woodward and Hudson, 1954). On the other hand in HEK293 cells, BRET remained at a basal level following addition of glucose (Figure 3B, right panel). This was not due to a difference in glucose uptake, which was similar in both cell types (Figure S3B). Thus, RESPYR allowed us to distinguish between cells that transport pyruvate into mitochondria for OXPHOS and those, such as HEK293 cells, that divert pyruvate to lactate and rely mainly on glycolysis.

To extend this analysis, we generated a range of cancer cell lines stably expressing RESPYR (143B, MCF7, HCT-116, HeLa, or MDA-MB231). We found that in all cases, the BRET signal increased in the presence of pyruvate but not in the presence of glucose (Figure S3C).

In order to confirm these observations independently of BRET, we labeled cells with ^{13}C-glucose and analyzed the amount of ^{13}C citrate after 0, 4, and 8 hr (Figure S3G) in both INS-1E cells, in which we could detect changes in BRET when the cells were provided with glucose, and HeLa cells, in which no significant increase in the BRET signal was detected in the presence of glucose. We found that while a substantial accumulation of ^{13}C-citrate was seen in INS-1E, no appreciable increase of ^{13}C-citrate could be detected in HeLa cells, even after 8 hr of labeling. Therefore, the lack of detectable citrate accumulation in HeLa cells, even using this sensitive isotope labeling assay, points to a low pyruvate uptake into mitochondria from cells grown in glucose-containing medium, which is in agreement with the results obtained using BRET. This observation is also fully consistent with the data previously reported by Yang et al. (2014a). Altogether, these results suggested that in the presence of glucose, either the concentration of pyruvate in cancer cells was significantly below the Km of pyruvate for the MPC and/or that the MPC or upstream processes were subjected to a glucose-induced negative control.

To distinguish between these two possibilities, we compared cytosolic pyruvate levels in INS-1E and HEK293 cells following growth in the presence of glucose using the previously described FRET sensor, Pyronic (San Martín et al., 2014). Pyronic is localized in the cytoplasm, and the FRET emission decreases in the presence of pyruvate, allowing us to monitor the cytosolic pyruvate concentration (Figure 3A). We found that in INS-1E, the levels of pyruvate were only slightly lower when cells were

incubated with glucose compared to pyruvate (Figure 3D, right panel). In contrast, in HEK293 cells, cytosolic pyruvate was detected when cells were exposed to pyruvate (Figure 3C, right panel, open red triangles) but not when incubated in the presence of glucose (Figure 3C, right panel, open blue squares). Thus, we conclude that the low levels of cytosolic pyruvate present in HEK293 cells exposed to glucose are at least partially responsible for the reduced MPC activity observed in these cells and in those cancer cells that rely mainly on glycolysis.

Inhibition of the MCT Leads to Increased Cytosolic Pyruvate Concentration and Activation of the MPC in Glycolytic Cells Exposed to Glucose

Based on the results above, we reasoned that in cancer cells, an increase in the concentration of cytosolic pyruvate might lead to MPC activation and an increase in OXPHOS. We hypothesized that decreasing the efflux of lactate by the MCTs should result in increased intracellular lactate, which in turn would favor accumulation of pyruvate. To investigate this possibility, cells were stimulated with glucose, and 10 min later the effect of AR-C155858 on the BRET response was assessed (Figures 3C and 3D). In HEK293 cells, glucose did not activate the MPC; however, following application of AR-C155858, a rapid increase in the BRET signal was observed (Figure 3C, left panel). Furthermore, this was associated with a rapid increase in cytosolic pyruvate as evidenced by a change in Pyronic-based FRET (Figure 3C, right panel). Thus MCT inhibition in HEK293 leads to accumulation of cytosolic pyruvate during aerobic glycolysis and increased MPC activity. In INS-1E cells, exposure to AR-C155858 accentuated the BRET and FRET changes observed after glucose stimulation (Figure 3D, blue symbols), also consistent with the notion that blocking the MCT leads to an increase in cytosolic pyruvate. As a control, when HEK293 and INS-1E cells were stimulated with pyruvate, inhibition of MCT1/2 by AR-C155858 reduced the cytosolic pyruvate concentration and thus reversed the pyruvate-induced increase in MPC activity (Figures 3C and 3D, red triangles). Some studies have suggested that MCT may also be localized in the mitochondria (Hashimoto et al., 2006; Hussien and Brooks, 2011). However in these experiments, any direct effect of AR-C155858 on mitochondria can be ruled out since the inhibitor did not affect BRET when added to isolated mitochondria (Figure 3E).

To investigate the functional consequences of increasing cytosolic pyruvate, we studied the oxygen consumption of HEK293. In the absence of AR-C155858, maximal oxygen consumption was almost three times higher when pyruvate was provided to cells compared to glucose (Figure 3F, black columns). However, following addition of the inhibitor, maximal oxygen consumption in glucose increased significantly and reached the same level as that observed in the presence of pyruvate (Figure 3F, gray columns). This effect of MCT inhibition on oxygen consumption was also observed in the absence of FCCP (Figure S3D), showing that pyruvate imported by MPC in cells incubated with glucose was metabolized in the TCA cycle. In contrast, MCT inhibition had the opposite effect on maximal oxygen consumption measured in cells exposed to pyruvate, consistent with the decrease in MPC activity induced by AR-C155858.

We then tested whether these observations could be extended to other glycolytic cells. Many cancer cells have been shown to express several MCT isoforms, including MCT1, MCT2, and MCT4. Moreover, unlike MCT1 and MCT2, MCT4 is insensitive to inhibition by AR-C155858 (Ovens et al., 2010). When RESPYR was expressed in 143B cells, AR-C155858 did not reduce MPC activity in the presence of pyruvate (Figure 3G), suggesting that in these cells, MCT4, or another AR-C155858-resistant carrier, transports monocarboxylates across the plasma membrane. Consistent with this notion, we observed that AR-C155858 did not increase MPC activity in the presence of glucose (Figure 3G). Similar observations were found in other cancer cell lines (HeLa, MCF7, and MDA-MB231) stably expressing RESPYR (data not shown). To investigate directly the role of MCT4 in AR-C155858-resistant pyruvate transport, we used the colon cancer cell line LS174T in which the MCT4 gene had been knocked out (Le Floch et al., 2011; Marchiq et al., 2015) ($MCT4^{-/-}$ cells, Figure 3H). In these cells, but not in the parental cell line, addition of AR-C155858 resulted in a significant increase of MPC activity in the presence of glucose, whereas MPC activity in the presence of pyruvate was decreased (Figure 3H, Figures S3E and S3F). Thus, RESPYR has enabled us to demonstrate a pro-oxidative function of the MCT1/2 inhibitor in MCT4 null glycolytic cells, which is associated with an increased intracellular pool of pyruvate (Marchiq et al., 2015).

Monitoring MPC Activity in Single Cells

To assess the ability of RESPYR to monitor MPC activity in real time in single cells, we compared the sensitivity to AR-C155858 of HEK293 and HeLa cells stably expressing RESPYR. HEK293 cells express MCT1/2 and are sensitive to AR-C155858, while HeLa cells also express MCT4, which is not inhibited by AR-C155858. To distinguish between the two cell lines, mCherry was expressed in HEK293 cells (Figure 4A). After addition of pyruvate, the MPC was activated and BRET increased in both cell lines as expected (Figure 4B and Figures S4A and S4B). In contrast, when cells were pre-incubated with AR-C155858, increased MPC activity was only visualized in HeLa cells (Figure 4C, arrow and Figures S4A and S4B), consistent with the results reported in the previous section.

DISCUSSION

Limitations

We have engineered a novel, genetically encoded biosensor of the MPC, named RESPYR, that is able to monitor MPC activity in real time. This sensor has allowed us to investigate the difference in MPC activity between cells undergoing aerobic glycolysis (HEK293 and cancer cells) and cells in which ATP generation is mainly provided by oxidative phosphorylation (INS-1E). Thus, RESPYR provides a powerful, non-invasive technology to monitor cellular energy metabolism and the shift in cancer cells from OXPHOS to aerobic glycolysis known as the Warburg effect. While the threshold sensitivity of RESPYR is likely to be less than other methods since it relies on real-time measurement of pyruvate flux through the MPC rather than the accumulation of pyruvate in mitochondria over time, it nevertheless offers several

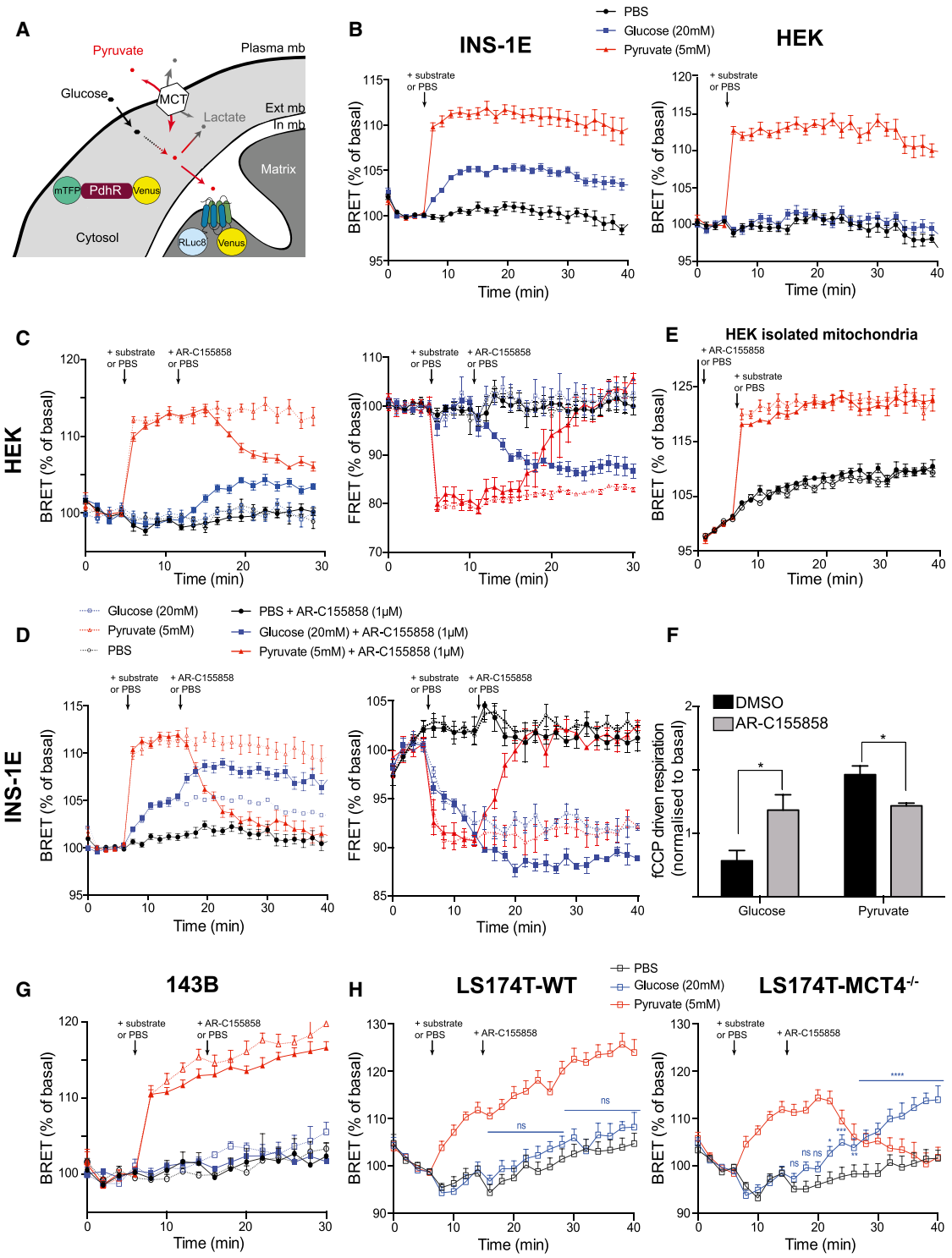

Figure 3. Effects of MCT Inhibition on Cell Metabolism

(A) Schematic representation of the subcellular localization of the biosensors RESPYR and Pyronic. MCT, monocarboxylate transporter; LDH, lactate dehydrogenase; Ext/In mb, mitochondrial external/inner membrane.

(B) BRET kinetics in either INS-1E (left panel) or HEK293 cells (right panel) transfected with RESPYR. At the times indicated by the arrows, cells were stimulated with PBS (black), 20 mM glucose (blue), or 5 mM pyruvate (red).

(legend continued on next page)

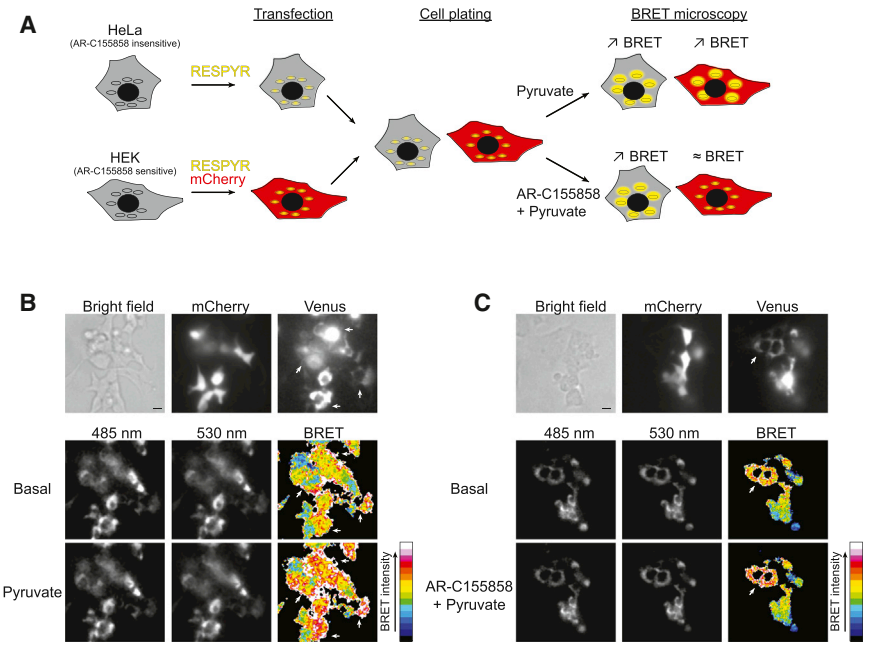

Figure 4. Visualizing MPC Activation in Single Cells

(A) Schematic representation of the experiment performed in (B) and (C) to visualize MPC activation by videomicroscopy of the variation in BRET. HEK293 cells express MCT1/2 and are sensitive to AR-C155858, while HeLa cells also express MCT4, which is not inhibited by AR-C155858. The two cell lines, stably expressing RESPYR, are transfected with either pCI-mCherry (HEK293) or vector alone (HeLa). 24 hr after transfection, the two cell lines are pooled and plated in 35 mm dishes. The two cell populations can be distinguished by excitation of mCherry. Following preincubation for 5 min with or without 1 μM AR-C155858, 5 mM pyruvate is added to each culture and BRET is recorded by videomicroscopy. In the presence of the MCT1/2 inhibitor, pyruvate-induced MPC activation should only be observed in HeLa cells.

(B and C) HEK293 cells were identified by direct excitation of mCherry, and all cells expressing RESPYR were identified by direct excitation of Venus. HeLa cells expressing RESPYR could thus be identified (arrows). Parallel cultures were left untreated (B) or exposed to 1 μM AR-C155858 (C). Following addition of coelenterazine h, images were acquired at 485 and 530 nm every 2 s for 10 min, before (basal) and after stimulation with 5 mM pyruvate. A 485/530 ratio image (BRET) is presented in pseudo-colors. In the presence of AR-C155858, pyruvate-induced MPC activation was only observed in HeLa cells (C, arrow). Scale bar, 10 μm.

See also Figure S4.

advantages for the study of glucose metabolism and OXPHOS: (i) it provides a direct measurement of mitochondrial pyruvate import in living cells with high temporal resolution; (ii) the demands on cell biomass of the assay are modest; (iii) using a suitable imaging platform, the procedure can be adapted to the analysis of single cells, thus providing high spatial resolution of MPC activity; and (iv) it can be scaled up to a high-throughput screening format in order to search for chemicals or other molecules able to modulate MPC activity. A potential limitation of the assay is that since it relies on ectopic expression of the two tagged subunits of the carrier, this may lead to excessive or non-uniform levels of expression of the subunits and/or to impairment of the conformational changes that underlie pyruvate transport. Our characterization of the biosensor thus far indicates that neither effect perturbs MPC activity. Cell lines stably expressing both subunits have been engineered using lentiviral infection, and lines can be selected in which both subunits are expressed at a similar level and at a level similar to that of the endogenous subunits. Furthermore co-immunoprecipitation experiments have shown that the engineered subunits are able to interact specifically with the appropriate endogenous partner, suggesting that C-terminal addition of the tags does not interfere with correct folding or topology of the subunits within the membrane. Experiments are currently in progress to incorporate the components of RESPYR into liposomes, and this will allow us to assess directly the affinity of pyruvate for the modified carrier.

RESPYR Reports Low MPC Activity in Cancer Cells Grown on Glucose

To investigate the Warburg effect, we have engineered five cancer cell lines that stably express the RESPYR components. In all of these cells, little or no change in BRET was observed in the presence of glucose, even at a high concentration (20 mM), and this is in marked contrast to our observations in INS-1E cells in which MPC is activated in glucose-containing media. All cell types tested expressed comparable levels of the BRET components (data not shown), and all responded similarly in medium

(C and D) Parallel cultures of HEK293 cells (C) and INS-1E cells (D) to study the kinetics of BRET (left panels, cells transfected with RESPYR) and FRET (right panels, cells transfected with Pyronic). At the times indicated (arrows), cells were stimulated with PBS (black), 20 mM glucose (blue), or 5 mM pyruvate (red) prior to treatment with 1 μM AR-C155858 (arrows).

(E) BRET kinetics measured in isolated mitochondria from HEK293 cells transfected with RESPYR. Cells were treated with 1 μM AR-C155858 (arrows) prior to treatment with PBS or 5 mM pyruvate. Symbols are as shown for (C) and (D).

(F) Maximal oxygen consumption rate in HEK293 cells after stimulation with 1 μM FCCP in the absence (black bars) or presence (gray bars) of 1 μM AR-C155858.

(G and H) BRET kinetics in 143B cells (G), LS174T cells (H, left panel), or LS174T-MCT4$^{-/-}$ cells (H, right panel) stably expressing RESPYR. Cells were treated as indicated in (C). Data were analyzed by a two-way ANOVA to determine difference between cells stimulated with PBS or glucose using Prism (GraphPad) software. *$p < 0.05$, **$p < 0.01$, ***$p < 0.005$, and ****$p < 0.001$. Data in (F) are mean and SEM of three independent experiments. Data in (B)–(D) are mean and SEM of one experiment with 4 wells per experiment and are representative of three independent experiments.

See also Figure S3.

containing pyruvate, indicating that the MPC is present and functional in all cases.

These observations therefore raise the important question of why the cancer cell lines tested respond differently to INS-1E cells upon stimulation with glucose. In an attempt to address this question, we have performed labeling studies with [U-^{13}C] glucose in which we show that the level of glucose-derived pyruvate that is converted into citrate in the TCA cycle is significantly lower in cancer cells than in INS-1E cells. These data are in agreement with a recent study by Yang et al. (2014a) who used a combined ^{13}C hyperpolarization and isotopomer analysis to address the fate of pyruvate in cells. These authors reported barely detectable levels of pyruvate entering into mitochondria when cancer cells were cultured in the presence of glucose, and they suggested that this may be due to reduced pyruvate dehydrogenase activity. Our results using RESPYR are fully consistent with the results of Yang et al. (2014a) obtained using cutting-edge metabolomics. In addition, we show that one of the reasons for this minimal pyruvate transport may be due to low levels of cytosolic pyruvate produced through glycolysis (see below). However, we do not exclude the possibility that other factors may also contribute to the reduced pyruvate uptake into mitochondria such as post-translational modifications of the carrier maybe through acetylation (Hebert et al., 2013), or perturbations downstream of the MPC, for example at the level of PDH as suggested by the results of Yang et al. (2014a), which may reduce the driving force for pyruvate import.

MCT as a Potential Target to Reverse the Warburg Effect

Pyruvate is produced through the highly regulated glycolytic flux and can be metabolized into alanine, malate, or lactate or transported across the outer mitochondrial membrane, probably through the voltage-dependent anion channel (VDAC). Using various cell types expressing RESPYR, we estimated that the affinity of pyruvate for the MPC is in the range from 225 μM to 452 μM, and these values are comparable to the intracellular pyruvate concentration reported previously (Bakowski and Parekh, 2007; Berman and Halperin, 1973; Zhu et al., 2010). Furthermore, using the pyruvate sensor Pyronic (San Martín et al., 2014), we found that the concentration of cytosolic pyruvate was much lower in glycolytic HEK293 cells than in INS-1E cells. We therefore wished to explore the importance of cytosolic pyruvate levels on MPC activity.

The MCTs are responsible for the bidirectional flux of pyruvate and lactate between the cytosol and the external environment (Halestrap, 2013). Thus, we reasoned that inhibition of the MCT in cells grown in glucose would result in an increased concentration of cytosolic lactate, feedback inhibition of LDH (Karlsson et al., 1974), and thus an increase in the level of cytosolic pyruvate. Pouyssegur and co-workers have recently shown that this is indeed the case (Marchiq et al., 2015), and their observations prompted us to test the effect of the MCT1/MCT2 inhibitor, AR-C155858, on the activity of the MPC. We found that inhibition of MCT1/MCT2 in HEK293 cells incubated with glucose increased cytosolic levels of pyruvate and that this resulted in a significant stimulation of the MPC activity. However, the MCT inhibitor had little effect on 143B cells, and other cancer cells (data not shown), probably because these cells also express MCT4, which is resistant to AR-C155858. Thus, efflux of lactate is not inhibited, and the intracellular pool of pyruvate does not increase. This was confirmed in experiments using the colon cancer cell line LS174T and the derivative of this line, LS174T-MCT4$^{-/-}$, in which MCT4 was genetically disrupted. While addition of AR-C155858 had no effect on the parental cell line after stimulation with glucose, a significant increase in MPC activity was observed in cells lacking MCT4 under the same conditions.

The Warburg effect seen in many cancer cells doubtless results from a combination of factors (Bayley and Devilee, 2012), among which modulation of MPC may be important. Indeed, recent data have shown that the MPC1 gene is deleted in various colon cancers and that re-introduction of MPC1 was able to repress the Warburg effect in these cells (Schell et al., 2014). Moreover, suppression of the MPC activity has a profound impact on cell metabolism and on the TCA cycle function (Vacanti et al., 2014; Yang et al., 2014b). Together, these studies indicate that modulating MPC activity in cancer cells may offer a potential approach to treating the disease. Here, we report that increasing pyruvate levels in the cytosol by using an inhibitor of the MCT may provide one possible strategy to activate MPC activity. From this proof of principle, we have now adapted our RESPYR assay to a high-throughput format, which will allow us to screen chemical or siRNA libraries for molecules able to modulate MPC activity.

EXPERIMENTAL PROCEDURES

Molecular Biology

Pyronic-pcDNA3.1(-) was obtained from Addgene. Plasmids encoding hMPC1-Flag and hMPC2-HA were generated by standard PCR cloning procedures using full-length cDNA clones obtained from the I.M.A.G.E consortium (hMPC1: clone 3452973; hMPC2: clone IRAMp995M0913Q). The amplified sequences were C-terminally fused to HA (YPYDVPDYA) or Flag (DYKDDDDK) tags by PCR and cloned into the pCI mammalian expression vector (Promega) or into the lentiviral vector pWPT (Addgene) for constitutive transgene expression.

For localization of the Venus fluorescent protein to the mitochondrial matrix (Mx-Venus) or the inter-membrane space (IMS-Venus), lentiviral plasmids were constructed in which the Venus coding sequence was fused downstream of the mitochondrial targeting sequences derived from the human CoxVIII or Smac genes, respectively, and assembled into the BamHI/SalI sites of the pWPT plasmid. Constructs were generated using the Gibson assembly protocol (New England BioLabs). Plasmids encoding hMPC1 and hMPC2 proteins tagged with RLuc8 and Venus were obtained as previously described (Compan et al., 2012). All constructs were confirmed by DNA sequencing.

Cell Culture and Reagents

AR-C18558 was obtained from Tocris; all others reagents were from Sigma. Mouse embryonic fibroblasts were obtained from embryonic day 12.5 (E12.5) embryos of an MPC1 genetrap mouse line (TIGM, clone OST39041) using standard procedures. The cells lines HEK293, MCF7, 143B, HCT-116, HeLa, MDA MB 231, and LS174T were maintained in DMEM supplemented with 10% fetal calf serum (FCS), 2 mM glutamine, and 1% pen/strep (Invitrogen). INS-1E cells (gift from P. Maechler) were maintained in RPMI1640 supplemented with 5% FCS, 2 mM glutamine, 50 μM β-mercaptoethanol, 25 mM HEPES, 1 mM pyruvate, and 1% pen/strep (all from Invitrogen).

Transfections were performed using Lipofectamine-LTX (Invitrogen). MEFs were electroporated using the Neon transfection system (Invitrogen) using the protocol supplied by the manufacturer. Stable cell lines were generated using a lentivirus-based procedure. Briefly, the DNA to be expressed was cloned into pWPT and co-transfected with the lentiviral packaging plasmids pMD2.G and psPAX2 (Addgene) into HEK293T cells by calcium phosphate

co-precipitation. Medium containing virus was collected 48 hr after transfection, centrifuged at 3,000 rpm for 5 min, and filtered (PES-glass, 0.45 μm pore). The viral supernatant was added to 70% confluent recipient cells, and transduction efficiency was estimated by immunofluorescence after 48 hr.

Isolation of Mitochondria-Rich Fraction, Co-immunoprecipitation, and Western Blotting

All steps were performed in the cold. Mitochondria were isolated from HEK293T cells stably expressing Mx-Venus, MPC1-Venus, IMS-Venus, or MPC2-Venus (4 confluent 150 mm plates per condition). Pellets containing mitochondria were weighed and resuspended in 4 volumes (w/v) of co-immunoprecipitation buffer (100 mM NaCl, 20 mM HEPES [pH 7.4], 5 mM EDTA, 0.2% Triton X-100, supplemented with complete protease inhibitor [Roche] and 1 mM benzamidine). Lysis was completed by rotation for 10 min, and the lysates were cleared by centrifugation at 1,500 rcf for 5 min. The pellet containing insoluble material (ins) was retained. Protein concentration in the supernatant was determined using the Bradford method and adjusted to 1 mg/ml by addition of co-immunoprecipitation buffer. This constituted the input fraction. 15 μl of GFP-nAb agarose beads (Allele Biotechnology) pre-washed in co-immunoprecipitation buffer were added to each input fraction, and co-immunoprecipitation was performed for 1 hr with continuous rotation. Beads were pelleted by centrifugation at 1,000 rcf for 1 min, and the supernatant (unbound fraction) was kept for western blot analysis. After washing 3 times in co-immunoprecipitation buffer, proteins were eluted by addition of LDS sample buffer (Invitrogen) supplemented with 10% β-mercaptoethanol and incubation at 95°C for 5 min. Samples were then loaded on 12% NuPage Bis-Tris gels (Invitrogen) and transferred onto 0.45 μM PVDF membranes. Western blot analysis was performed using antibodies directed against Tom20 (sc-11415, Santa Cruz Biotechnology), MPC1 (HPA045119, Sigma), MPC2 (mouse monoclonal, home-made), and GFP (11814460001, Roche).

Cell Proliferation

Cells were seeded in 12-well culture plates at 2.10^4 cells/well. At different times following cell plating (24 hr, 48 hr, 72 hr, and 96 hr), cells were resuspended using trypsin and counted using a Neubauer chamber.

Oxygen Consumption

Oxygen consumption measurements were performed using the Seahorse XFe24 Flux Analyzer and the XF cell Mito stress kit (Seahorse Biosciences) as previously described (Divakaruni et al., 2013). Briefly, 24-well plates were seeded with 40,000 cells/well and incubated at 37°C. After 24 hr, cells were incubated with DMEM (Sigma D5030) (pH7.4) containing 5 mM glucose and 0.5 mM dichloroacetate for 1 hr at 37°C without CO_2. Cells were then exposed sequentially to DMSO or AR-C18558 (1 μM), glucose (20 mM) or pyruvate (5 mM), FCCP (1 μM), and rotenone (1 μM)/antimycin (1 μM). The values represent averages of 4 different wells.

Where indicated, OCR was measured in permeabilized cells using 1 nM XF PMP in MAS Buffer (Seahorse Biosciences) with 5 mM pyruvate, 2 mM dichloroacetate, 0.5 mM malate, and 1 μM oligomycin. Cells were sequentially exposed to 0.5 μM FCCP, 1 μM rotenone/10 mM succinate, and 1 μM antimycin.

BRET Measurement

Cells were plated in white 96-well plates 48 hr before recording. Cells were washed with PBS-CM (PBS supplemented with 1 mM $CaCl_2$ and 0.5 mM $MgCl_2$), and readings were performed 5 min after addition of 5 μM coelenterazine h substrate (Invitrogen). Signals were detected with two filter settings (R-Luc8 filter, 460 ± 40 nm; and Venus filter, 528 ± 20 nm) at 37°C using the Synergy 2 plate reader (Biotek). The BRET value was defined as the difference between the emission at 528 nm/460 nm of co-transfected R-Luc8 and Venus fusion proteins (MPC2-R + MPC1-V) and the emission at 528 nm/460 nm of the R-Luc8 fusion protein alone (MPC2-R). Results were expressed in milliBRET units (mBU). For saturation curves, a constant amount of the plasmid expressing the R-Luc8 tagged protein was co-transfected with increasing quantities of the plasmid expressing the Venus-tagged protein. BRET signals were determined as described above. The amount of Venus- and R-Luc8-tagged proteins was determined in parallel plates by reading at 528 nm after excitation at 460 nm (Venus) and at 460 nm in the presence of coelenterazine h (RLuc8).

Where indicated, cells were permeabilized with 1 nM XF PMP prior to adding 5 μM coelenterazine h substrate.

BRET Microscopy

Single-cell BRET recording was performed, as described previously (Compan et al., 2012). Briefly, HEK and HeLa cells were transfected in 35 mm dishes as described above. 24 hours later, both cell lines were mixed and plated in 35 mm dishes (μ-Dish from Ibidi). BRET imaging studies were performed at 37°C using an Olympus LV200 equipped with a 60×/1.42 Oil objective. Transfected cells were identified using filters to excite Venus (exciter SP480, emitter HQ530/30) and mCherry (exciter HQ560/20, emitter HQ600/50). Coelenterazine h (20 μM) was applied 7 min before acquisition. Images were collected using a Hamamatsu ImageEM camera (equipped with a cooled [−80°C] CCD detector). Sequential acquisitions of 1 or 5 s (depending on sensor expression) were performed with emission filters D485/25 nm and HQ530/30 nm to select em485 and em530 wavelengths, respectively. Acquisition and analysis were performed by Cellsense (Olympus) and ImageJ (NIH) software, respectively. BRET signals were represented using a continuous 256-pseudocolor look-up table, as displayed in the figures.

FRET Measurement

Cells were prepared as described above for BRET. FRET experiments were performed at 37°C using the Synergy 3 plate reader (Biotek). Signals were recorded at 485 nm and 535 nm after excitation at 425 nm. The FRET was defined as the ratio between the emission at 485 nm and 535 nm.

Immunofluorescence

For mitochondria staining, HeLa cells were incubated for 10 min at 37°C with Mitotracker (Invitrogen, 1:1,000) diluted in complete medium before washing for a further 10 min in complete medium. Cells were washed twice with PBS, fixed with 4% formaldehyde, 4% sucrose in PBS for 5 min at room temperature, and then washed three times with PBS before incubation in ice-cold acetone for 5 min. All coverslips were mounted on slides with ProLong Gold Antifade Reagent (Invitrogen). Images were acquired with a Zeiss Axiophot microscope equipped with a 63×/1.4 Plan Apo objective and a QImaging Retiga Ex camera.

Metabolomics

HEK293 cells and INS-1E cells were cultured in 6-well plates in medium containing serum and supplemented with 20 mM [U-^{13}C]glucose. Metabolites were extracted twice from plates in the presence of hot (75°C) 70% ethanol. Targeted analysis of citrate levels and labeling was performed by ion-pairing, reverse-phase, ultra-performance liquid chromatography-tandem mass spectrometry on a Thermo Quantum Ultra instrument (Thermo Scientific) (Buescher et al., 2010).

Glucose Uptake

Glucose uptake studies were performed using the fluorescent glucose analog, 2-NBD-Glucose (2-NBDG, Invitrogen). Briefly, cells grown in 96-well plates were washed with PBS and incubated with 2-NBDG (100 μM) for different times as indicated in the figure legend. Cells were washed with PBS, and fluorescence was recorded at 535 nm after excitation at 485 nm using the Synergy 3 monochromator plate reader (Biotek).

Statistical Analysis

Data points are expressed as the mean ± SEM using the number of replicates indicated in the figure legends. Unless otherwise indicated, the difference between groups was analyzed by unpaired Student's t test using Prism (GraphPad) software. *$p < 0.05$, **$p < 0.01$, and ***$p < 0.001$.

SUPPLEMENTAL INFORMATION

Supplemental Information includes four figures and can be found with this article online at http://dx.doi.org/10.1016/j.molcel.2015.06.035.

AUTHOR CONTRIBUTIONS

V.C. and J.-C.M. conceived the study and wrote the final manuscript. I.M. and J.P. provided the LS174T cell lines and contributed to the final version of the manuscript. S.P. performed, analyzed, and interpreted experiments of oxygen consumption and cell proliferation. B.V. designed and performed experiments of MPC co-immunoprecipitation. S.P. and P.K. performed metabolomic experiments, and P.K. and N.Z. analyzed the results. V.C. designed, executed, and analyzed all other experiments with the contribution of S.P. All authors critically reviewed the manuscript.

ACKNOWLEDGMENTS

We thank Dr. K. Maundrell for critical reading of the manuscript, Dr. P. Maechler (CMU, Geneva) for kindly providing us with the INS-1E cells, and C. Bauer and J. Bosset of the Bioimaging center of Geneva for their help during single-cell BRET recording. V.C. was supported by a Marie Curie Intra European Fellowship and by the Institut National de la Santé et de la Recherche Médicale. I.M. was supported by a fellowship from the Ligue Nationale Contre le Cancer and J.P. Lab by Ligue Nationale Contre le Cancer (Equipe labellisée LNCC). This work was supported by the Swiss National Science Foundation (31993A-141068/1), Sinergia (CRSII3_147637) IGE3, the State of Geneva, and the Ligue Genevoise Contre le Cancer.

Received: February 2, 2015
Revised: May 22, 2015
Accepted: June 26, 2015
Published: August 6, 2015

REFERENCES

Bakowski, D., and Parekh, A.B. (2007). Regulation of store-operated calcium channels by the intermediary metabolite pyruvic acid. Curr. Biol. *17*, 1076–1081.

Bayley, J.P., and Devilee, P. (2012). The Warburg effect in 2012. Curr. Opin. Oncol. *24*, 62–67.

Bender, T., Pena, G., and Martinou, J.C. (2015). Regulation of mitochondrial pyruvate uptake by alternative pyruvate carrier complexes. EMBO J. *34*, 911–924.

Berman, B.G., and Halperin, M.L. (1973). Effect of insulin on pyruvate metabolism in epididymal adipose tissue of the rat. Correlation of intracellular pyruvate contents and pyruvate dehydrogenase activity. Biochem. J. *134*, 885–889.

Bricker, D.K., Taylor, E.B., Schell, J.C., Orsak, T., Boutron, A., Chen, Y.C., Cox, J.E., Cardon, C.M., Van Vranken, J.G., Dephoure, N., et al. (2012). A mitochondrial pyruvate carrier required for pyruvate uptake in yeast, Drosophila, and humans. Science *337*, 96–100.

Buescher, J.M., Moco, S., Sauer, U., and Zamboni, N. (2010). Ultrahigh performance liquid chromatography-tandem mass spectrometry method for fast and robust quantification of anionic and aromatic metabolites. Anal. Chem. *82*, 4403–4412.

Cairns, R.A., Harris, I.S., and Mak, T.W. (2011). Regulation of cancer cell metabolism. Nat. Rev. Cancer *11*, 85–95.

Compan, V., Baroja-Mazo, A., Bragg, L., Verkhratsky, A., Perroy, J., and Pelegrin, P. (2012). A genetically encoded IL-1β bioluminescence resonance energy transfer sensor to monitor inflammasome activity. J. Immunol. *189*, 2131–2137.

DeBerardinis, R.J., Lum, J.J., Hatzivassiliou, G., and Thompson, C.B. (2008). The biology of cancer: metabolic reprogramming fuels cell growth and proliferation. Cell Metab. *7*, 11–20.

Dietmair, S., Hodson, M.P., Quek, L.E., Timmins, N.E., Gray, P., and Nielsen, L.K. (2012). A multi-omics analysis of recombinant protein production in Hek293 cells. PLoS ONE *7*, e43394.

Divakaruni, A.S., Wiley, S.E., Rogers, G.W., Andreyev, A.Y., Petrosyan, S., Loviscach, M., Wall, E.A., Yadava, N., Heuck, A.P., Ferrick, D.A., et al. (2013). Thiazolidinediones are acute, specific inhibitors of the mitochondrial pyruvate carrier. Proc. Natl. Acad. Sci. USA *110*, 5422–5427.

Halestrap, A.P. (2013). Monocarboxylic acid transport. Compr Physiol *3*, 1611–1643.

Hashimoto, T., Hussien, R., and Brooks, G.A. (2006). Colocalization of MCT1, CD147, and LDH in mitochondrial inner membrane of L6 muscle cells: evidence of a mitochondrial lactate oxidation complex. Am. J. Physiol. Endocrinol. Metab. *290*, E1237–E1244.

Hebert, A.S., Dittenhafer-Reed, K.E., Yu, W., Bailey, D.J., Selen, E.S., Boersma, M.D., Carson, J.J., Tonelli, M., Balloon, A.J., Higbee, A.J., et al. (2013). Calorie restriction and SIRT3 trigger global reprogramming of the mitochondrial protein acetylome. Mol. Cell *49*, 186–199.

Henry, O., Jolicoeur, M., and Kamen, A. (2011). Unraveling the metabolism of HEK-293 cells using lactate isotopomer analysis. Bioprocess Biosyst. Eng. *34*, 263–273.

Herzig, S., Raemy, E., Montessuit, S., Veuthey, J.L., Zamboni, N., Westermann, B., Kunji, E.R., and Martinou, J.C. (2012). Identification and functional expression of the mitochondrial pyruvate carrier. Science *337*, 93–96.

Hiller, K., and Metallo, C.M. (2013). Profiling metabolic networks to study cancer metabolism. Curr. Opin. Biotechnol. *24*, 60–68.

Hsu, P.P., and Sabatini, D.M. (2008). Cancer cell metabolism: Warburg and beyond. Cell *134*, 703–707.

Hussien, R., and Brooks, G.A. (2011). Mitochondrial and plasma membrane lactate transporter and lactate dehydrogenase isoform expression in breast cancer cell lines. Physiol. Genomics *43*, 255–264.

Jang, M., Kim, S.S., and Lee, J. (2013). Cancer cell metabolism: implications for therapeutic targets. Exp. Mol. Med. *45*, e45.

Karlsson, J., Hultén, B., and Sjödin, B. (1974). Substrate activation and product inhibition of LDH activity in human skeletal muscle. Acta Physiol. Scand. *92*, 21–26.

Le Floch, R., Chiche, J., Marchiq, I., Naiken, T., Ilc, K., Murray, C.M., Critchlow, S.E., Roux, D., Simon, M.P., and Pouysségur, J. (2011). CD147 subunit of lactate/H+ symporters MCT1 and hypoxia-inducible MCT4 is critical for energetics and growth of glycolytic tumors. Proc. Natl. Acad. Sci. USA *108*, 16663–16668.

Locasale, J.W., and Cantley, L.C. (2011). Metabolic flux and the regulation of mammalian cell growth. Cell Metab. *14*, 443–451.

Marchiq, I., Le Floch, R., Roux, D., Simon, M.P., and Pouyssegur, J. (2015). Genetic disruption of lactate/H+ symporters (MCTs) and their subunit CD147/BASIGIN sensitizes glycolytic tumor cells to phenformin. Cancer Res. *75*, 171–180.

Michelakis, E.D., Sutendra, G., Dromparis, P., Webster, L., Haromy, A., Niven, E., Maguire, C., Gammer, T.L., Mackey, J.R., Fulton, D., et al. (2010). Metabolic modulation of glioblastoma with dichloroacetate. Sci. Transl. Med. *2*, 31ra34.

Ovens, M.J., Davies, A.J., Wilson, M.C., Murray, C.M., and Halestrap, A.P. (2010). AR-C155858 is a potent inhibitor of monocarboxylate transporters MCT1 and MCT2 that binds to an intracellular site involving transmembrane helices 7-10. Biochem. J. *425*, 523–530.

Papa, S., Francavilla, A., Paradies, G., and Meduri, B. (1971). The transport of pyruvate in rat liver mitochondria. FEBS Lett. *12*, 285–288.

San Martín, A., Ceballo, S., Baeza-Lehnert, F., Lerchundi, R., Valdebenito, R., Contreras-Baeza, Y., Alegría, K., and Barros, L.F. (2014). Imaging mitochondrial flux in single cells with a FRET sensor for pyruvate. PLoS ONE *9*, e85780.

Schell, J.C., Olson, K.A., Jiang, L., Hawkins, A.J., Van Vranken, J.G., Xie, J., Egnatchik, R.A., Earl, E.G., DeBerardinis, R.J., and Rutter, J. (2014). A role for the mitochondrial pyruvate carrier as a repressor of the Warburg effect and colon cancer cell growth. Mol. Cell *56*, 400–413.

Spacek, T., Santorová, J., Zacharovová, K., Berková, Z., Hlavatá, L., Saudek, F., and Jezek, P. (2008). Glucose-stimulated insulin secretion of insulinoma INS-1E cells is associated with elevation of both respiration and mitochondrial membrane potential. Int. J. Biochem. Cell Biol. *40*, 1522–1535.

Vacanti, N.M., Divakaruni, A.S., Green, C.R., Parker, S.J., Henry, R.R., Ciaraldi, T.P., Murphy, A.N., and Metallo, C.M. (2014). Regulation of substrate utilization by the mitochondrial pyruvate carrier. Mol. Cell *56*, 425–435.

Vander Heiden, M.G., Cantley, L.C., and Thompson, C.B. (2009). Understanding the Warburg effect: the metabolic requirements of cell proliferation. Science *324*, 1029–1033.

Vanderperre, B., Bender, T., Kunji, E.R., and Martinou, J.C. (2015). Mitochondrial pyruvate import and its effects on homeostasis. Curr. Opin. Cell Biol. *33*, 35–41.

Woodward, G.E., and Hudson, M.T. (1954). The effect of 2-desoxy-D-glucose on glycolysis and respiration of tumor and normal tissues. Cancer Res. *14*, 599–605.

Yang, C., Harrison, C., Jin, E.S., Chuang, D.T., Sherry, A.D., Malloy, C.R., Merritt, M.E., and DeBerardinis, R.J. (2014a). Simultaneous steady-state and dynamic 13C NMR can differentiate alternative routes of pyruvate metabolism in living cancer cells. J. Biol. Chem. *289*, 6212–6224.

Yang, C., Ko, B., Hensley, C.T., Jiang, L., Wasti, A.T., Kim, J., Sudderth, J., Calvaruso, M.A., Lumata, L., Mitsche, M., et al. (2014b). Glutamine oxidation maintains the TCA cycle and cell survival during impaired mitochondrial pyruvate transport. Mol. Cell *56*, 414–424.

Zhu, A., Romero, R., and Petty, H.R. (2010). A sensitive fluorimetric assay for pyruvate. Anal. Biochem. *396*, 146–151.